Comparative assessment of brain MR image segmentation algorithms and their impact on partial volume effect correction in PET

Habib Zaidi, Torsten Ruest, Frédéric Schoenahl and Marie-Louise Montandon

Division of Nuclear Medicine, Geneva University Hospital, CH 1211 Geneva, Switzerland

Reprints: *habib.zaidi@hcuge.ch*

INTRODUCTION:

➢Magnetic Resonance Imaging (MRI)-guided partial volume effect correction (PVC) in PET is now a well established approach to compensate the large bias in the estimate of regional radioactivity concentration, especially for small structures.

➢The accuracy of the algorithms developed so far are, however, largely dependent on the performance of segmentation algorithms, partitioning MR brain images into its main compartments, namely gray matter (GM), white matter (WM), and cerebrospinal fluid (CSF).

AIM

Compare the effect of **three brain MRI segmentation algorithms** using simulated and clinical brain MR data, and subsequently assess their **impact on partial volume effect correction** in ^{18}F-FDG and ^{18}F-DOPA brain PET imaging

METHOD:

MR brain segmentation algorithms:

- **SPM2:** MR image segmentation algorithm bundled in the Statistical Parametric Mapping (SPM2) package (Ashbuhner and Friston, 1997, 2000).
- **EMS:** Expectation Maximization Segmentation algorithm (Van Leemput et al. (1999).
- **HBSA:** Histogram-based Segmentation Algorithm incorporating an Expectation Maximization approach (Kovacevic et al. 2002).

Clinical and digital brain phantom studies:

➢Images of digital brain phantoms were simulated by means of a dedicated MRI simulator (Kwan *et al.* 1999), using a SFLASH sequence (TR=15ms, TE=4.4ms, FA=25°). Realistic brain phantoms were generated with randomly distributed noise with levels of 3%, 5%, 7%, and 9% and with intensity non-uniformity (INU) of 0%, 20% and 40%. Ten volumes were generated for each combination of noise and INU.

➢Clinical brain scans of 10 patients referred to the Nuclear Medicine Division of Geneva University Hospital for detection of epileptic foci with seizures using [^{18}F]-FDG PET and T1-weighted MRI were selected from the database and used for clinical evaluation of the impact of MR-segmentation algorithms.

➢PET scanning was performed using the ECAT ART scanner (CTI/Siemens) operated in fully 3D mode whereas the anatomy of each patient was defined using high-resolution 3D T1-weighted volumetric MR scanning performed with a 1.5-Tesla Eclipse scanner (Philips Medical Systems).

Partial volume effect correction algorithm (GTM):

➢The geometric transfer matrix (GTM) method calculates corrected estimates without *a priori* knowledge on any activity level by partial volume factors are computed from simulation of the noise-free regional point spread function (*RSF*) images and sampling with a user-defined set of RoIs (Rousset *et al.* 1998). The number of RoIs must be equal to the number of tissue components identified in the tracer model in order to provide a full-rank GTM.

RESULTS:

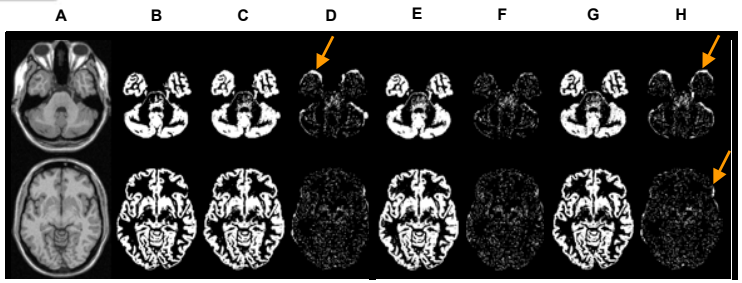

Figure 1. Gray matter segmentation of simulated MRI brain phantoms. **A:** original MRI; **B:** Ground truth; **C:** SPM; **D:** |B-C|; **E:** EMS; **F:** |B-E|; **G:** HBSA; **H:** |B-G|.

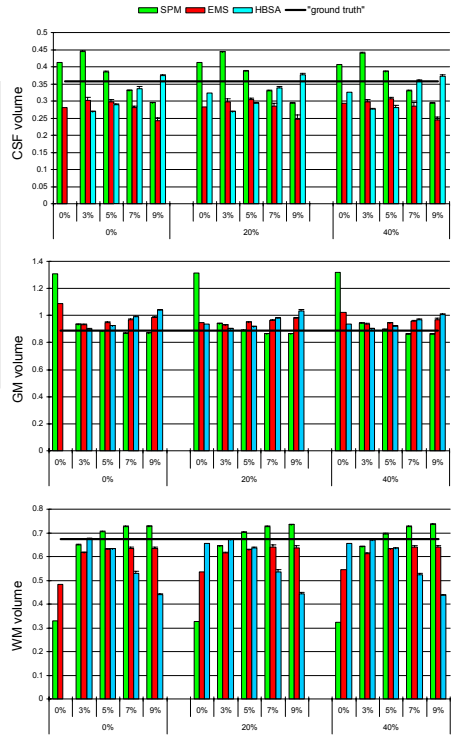

Figure 2. Volumes of segmented binarized brain tissues. Inner values of the x-axis correspond to the noise level, outer values correspond to the INU. Dark line corresponds to the binarized "ground truth" volumes. GM: 887091 mm^3; WM: 674662 mm^3; CSF: 356666 mm^3 (volumes are reported in 10^6 mm^3).

Table 1. Relative difference (%) between segmentation algorithms calculated on the basis of the first called algorithm. I: bad brain extraction (BET), II: infant data, a: data just used for SPM-HBSA analysis, b: segmentation error.

	GM uncorrected			GM corrected		
	EMS-HBSA	SPM-EMS	SPM-HBSA	EMS-HBSA	SPM-EMS	SPM-HBSA
1[a]	—	—	3.85	—	—	2.25
2[b]	1.32	0.76	0.57	7.77	0.82	8.52
3	1.63	0.83	0.79	7.99	1.31	9.19
4	0.31	0.04	0.35	6.02	4.79	10.52
5[II]	1.49	0.49	1.01	8.24	1.15	7.18
6	0.31	0.11	0.20	7.94	1.44	9.26
7	0.12	0.02	0.15	7.06	1.00	7.98
8	0.10	0.41	0.51	6.49	2.10	8.45
9[I]	3.19	1.09	4.32	13.76	3.74	9.51
10[a]	—	—	1.54	—	—	8.97
11	0.01	0.34	0.34	6.50	4.51	10.71
	WM uncorrected			**WM corrected**		
	EMS-HBSA	SPM-EMS	SPM-HBSA	EMS-HBSA	SPM-EMS	SPM-HBSA
1[a]	—	—	1.38	—	—	4.71
2[b]	1.30	0.86	2.17	9.95	1.52	8.28
3	1.93	1.17	0.78	2.89	0.21	3.10
4	4.38	0.08	4.29	15.77	3.18	12.08
5[II]	5.83	1.01	4.76	24.01	6.16	16.37
6	1.44	1.30	0.16	0.43	0.09	0.34
7	2.33	1.01	3.37	11.55	1.24	10.17
8	2.59	0.69	3.29	12.07	3.56	8.07
9[I]	3.42	1.48	1.99	12.42	0.19	12.59
10[a]	—	—	0.69	—	—	8.53
11	0.37	0.35	0.72	5.90	0.93	4.92

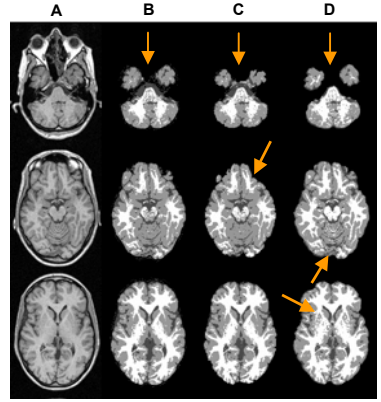

Figure 3. Segmentation of clinical MRI data. **A:** Original MRI, **B:** SPM; **C:** EMS and **D:** HBSA. White is WM, light dark corresponds to GM, and dark gray to CSF. Arrows show discrepancies between segmentation results.

CONCLUSION:

➢The results of digital MRI phantom studies suggest that the use of the HBSA produces best performance from WM classification. For GM classification, it is suggested to use the EMS.

➢Segmentation performed on clinical MRI show partly quite substantial differences, especially where lesions are present. For the particular case of PVC, the SPM and EMS show very similar results and may be used interchangeably. The use of the HBSA is not recommended for PVC.

REFERENCES:

Ashburner J. and Friston K. (1997) Multimodal image coregistration and partitioning - a unified framework. Neuroimage **6:** 209-217
Ashburner J. and Friston K. (2000) Voxel-based morphometry - the methods. Neuroimage **11:** 805-821
Kovacevic N. et al. (2002) A robust method for extraction and automatic segmentation of brain images. Neuroimage **17:** 1087-1100
Kwan RK. et al. (1999) MRI simulation-based evaluation of image-processing and classification methods. IEEE Trans Med Imaging **18:** 1085-1097
Rousset OG. et al. (1998) Correction for partial volume effects in PET: principle and validation. J Nucl Med **39:** 904-911
Van Leemput K. et al. (1999) Automated model-based tissue classification of MR images of the brain. IEEE Trans Med Imaging **18:** 897-908

Acknowledgements:

This work was supported by the Swiss National Science Foundation under grant SNSF 3152A0-102143 and and the Research and Development Foundation of Geneva University Hospital under grant PRD-04-1-08.